ESA Contract Report

SMOS ESL contract 4000130567/20/I-BG

Contract Report to the European Space Agency

Annual SMOS brightness temperature monitoring report

Authors: Pete Weston and Patricia de Rosnay
Contract officer: Raffaele Crapolicchio

January 2021

Series: ECMWF ESA Contract Report Series

A full list of ECMWF Publications can be found on our website under:
http://www.ecmwf.int/en/publications

Contact: library@ecmwf.int

European Centre for Medium-Range Weather Forecasts, Shinfield Park, Reading, RG2 9AX, UK

Abbreviations

BUFR ..... Binary Universal Form for the Representation of meteorological data
CMEM ..... Community Microwave Emissivity Modelling platform
ECMWF ..... European Centre for Medium-range Weather Forecasts
ESA ..... European Space Agency
IFS ..... Integrated Forecast System
NRT ..... Near Real Time
NWP ..... Numerical Weather Prediction
RFI ..... Radio Frequency Interference
SMOS ..... Soil Moisture and Ocean Salinity
Tb ..... Brightness Temperature

1. Introduction

This document provides an annual summary of the performance of the European Space Agency (ESA) Soil Moisture and Ocean Salinity (SMOS) brightness temperature (Tb) monitoring run routinely at the European Centre for Medium-range Weather Forecasts (ECMWF). The period covered is September 2019 to August 2020. Several different monitoring plots are presented, and notable features are described in detail. Also, potential improvements to the monitoring system are proposed.

2. Annual SMOS monitoring results

Routine operational monitoring of SMOS observations from the NRT BUFR product is performed at ECMWF. The SMOS measured brightness temperatures are compared to short-term numerical weather prediction (NWP) forecasts transformed into brightness temperatures using the Community Microwave Emissivity Model (CMEM). The differences between these two quantities are known as first-guess departures and statistics of these first-guess departures are accumulated and plotted routinely.

The samples used to produce the plots can be filtered by area, including global, Northern and Southern Hemispheres, as well as loose definitions of the continents: Europe (120°W-120°E, 35°N-77.5°N), Asia (0°W-120°W, 40°N-82.5°N), North America (120°E-0°E, 20°N-77.5°N), South America (120°E-0°E, 40°S-17.5°N) and Australia (0°E-120°W, 47.5°S-7.5°S). This section focuses on global statistics.

Also, the plots are produced separately for data:

- Over sea or over land
- With different incidence angles: 30°, 40° or 50°
- With different polarisations: H (XX) or V (YY) at the SMOS antenna reference frame

A selection of different options for surface type, incidence angles and polarisations are presented and the full set of plots are available via FTP at ftp://dpgswebserver-2.smos.eo.esa.int/SMOS_ESL2020/Task-5/Annual_Monitoring/2020/All_plots.zip.

A thorough introduction to the monitoring system can be found in Weston and de Rosnay (2020) and examples of the plots produced can be seen at https://www.ecmwf.int/en/forecasts/quality-our-forecasts/monitoring/smos-monitoring. In this section each of the different types of plots produced as part of the SMOS monitoring system are presented and any notable features are highlighted to be investigated in more detail in the following sections.

2.1. Time series

Statistics are plotted as lines against time on the x-axis for the full twelve-month period with statistics accumulated in 12 hour chunks. The statistics plotted are mean and standard deviation of first-guess departures, the mean observed and first-guess brightness temperatures and number of observations. These plots allow global trends and jumps in the statistics to be identified.

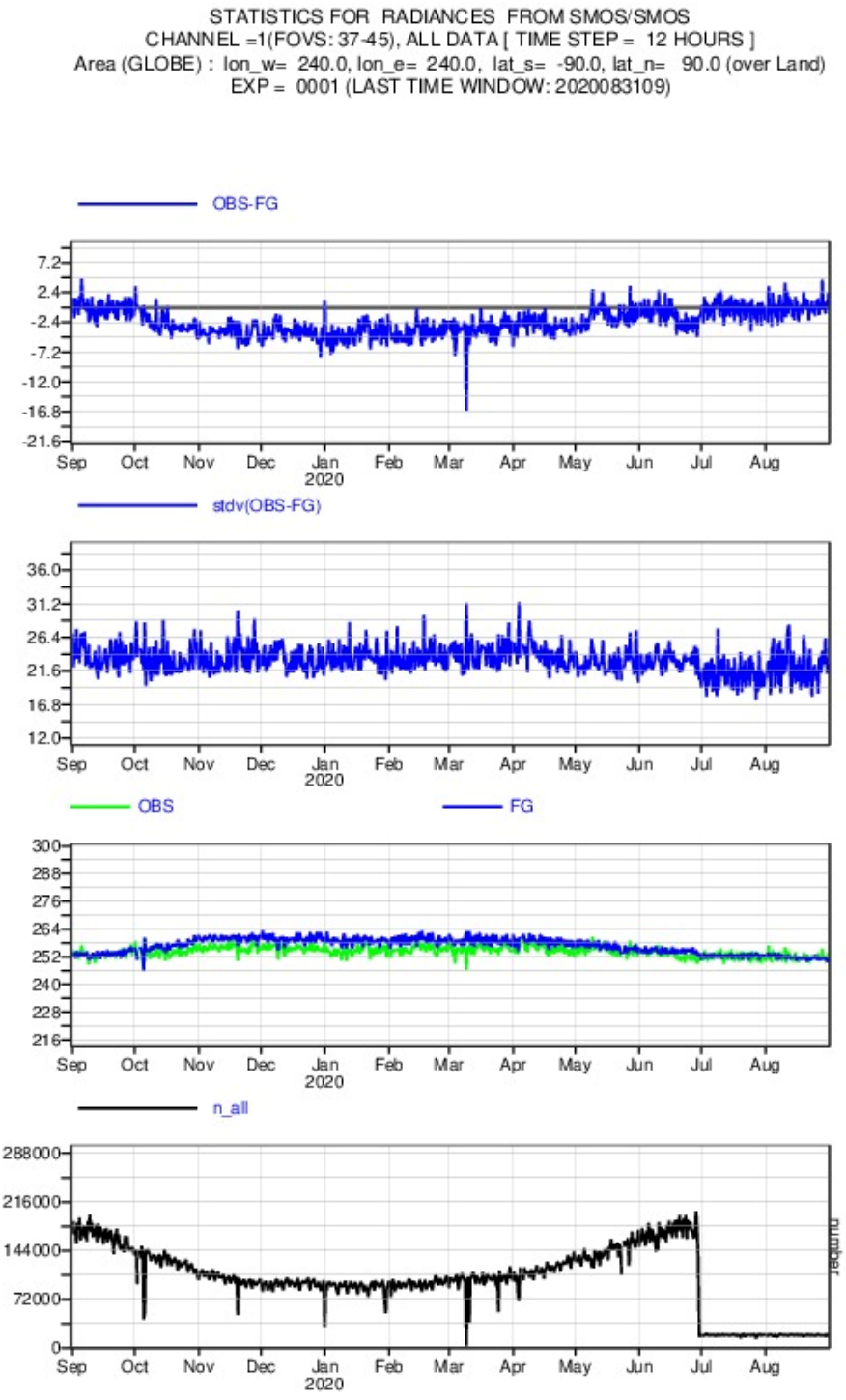

Figure 1: Time series of mean first-guess departures (upper panel), standard deviation of first-guess departures (2nd panel), mean observed and first-guess values (3rd panel) and number of observations (lower panel). Statistics are accumulated for SMOS observations over land at 40° incidence angle, H polarisation and cover 1st September 2019 to 31st August 2020

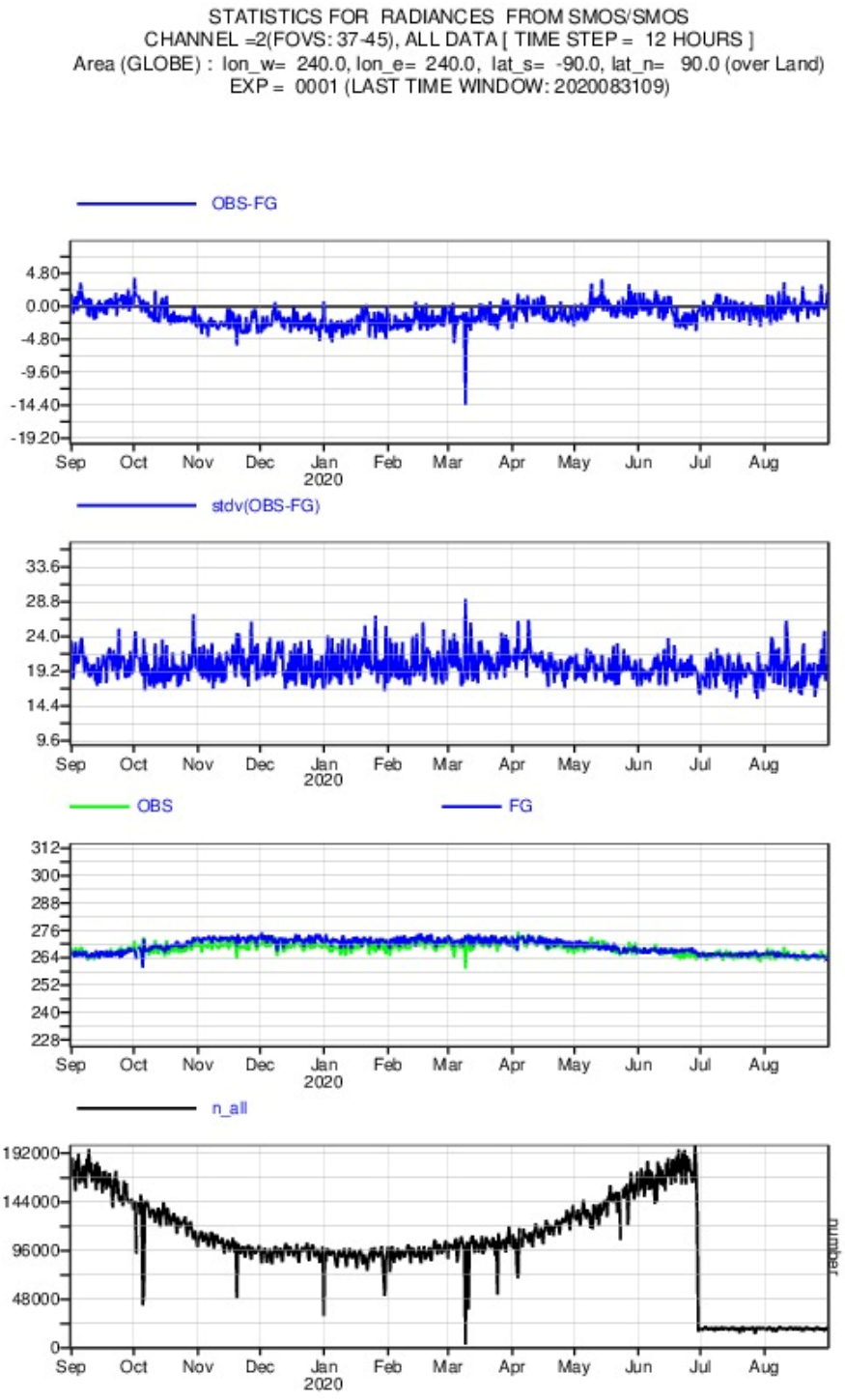

Figure 2: As figure 1 but for SMOS observations with V polarisation

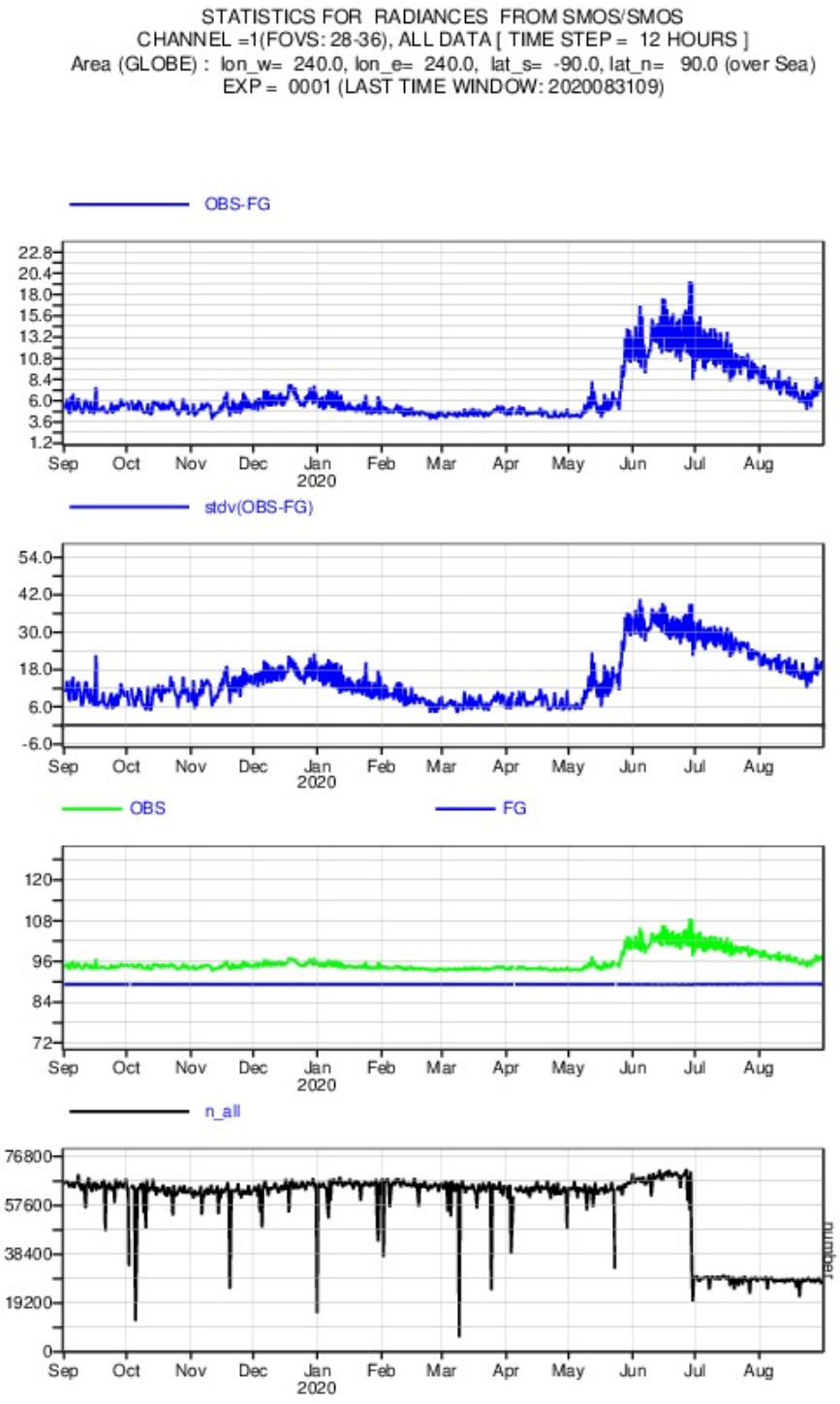

Figure 3: As figure 1 but statistics are accumulated for SMOS observations over ocean at 30° incidence angle, H polarisation and cover 1st September 2019 to 31st August 2020

Figures 1 and 2 show that the first-guess departure statistics over land are generally very stable over the year. The mean first-guess departures mostly vary between ±5K for H polarisations and ±3K for V polarisations with only very occasional global mean values outside of this range. The standard

deviation of first-guess departures have slightly more day-to-day variability but generally stay close to a value of 24K for H polarisations and 20K for V polarisations. The apparent slightly better performance of the V polarisations over the H polarisations could be due to an instrument effect but it could also be due to differing performance of the CMEM observation operator used to convert the model soil moisture to brightness temperature. It should be noted that the first guess departures presented here do not have a bias correction applied and the statistics are consistent with those found between 2010 and 2016 without bias correction in de Rosnay et al (2020). The largest variation is seen in the number of observations monitored. Between September 2019 and December 2019 there is a significant reduction of almost 50% in the number of observations monitored. This is due to the Northern hemisphere winter and many observations over Northern hemisphere land surfaces being screened out due to frozen soil and snow. At the same time there is a corresponding negative shift in the mean first-guess departures, see section 2.3 for more discussion on this. Between March 2020 and June 2020 this trend is reversed as the Northern hemisphere summer starts and the land thaws out. On 30th June 2020 there is a sudden very large reduction in the number of SMOS observations monitored. This coincides with the implementation of the latest ECMWF model cycle, 47r1, and a corresponding reduction in the resolution that the monitoring is run at. See section 3.1 for more details.

Figure 3 shows that there is larger annual variability in the first-guess departure statistics over ocean than over land. The increases in both mean and standard deviation of first-guess departures around December 2019 to February 2020 and June 2020 to August 2020 are both caused by sub-optimal frozen surface screening where observations over sea-ice with much larger first-guess departures contaminate the global sample. See sections 3.2 and 4.1 for more details. The number of observations between September 2019 and June 2020 is much more stable over ocean than over land, this is also a sign that the frozen surface screening over ocean is sub-optimal. A similar sudden reduction on 30th June 2020 is seen over ocean as over land, again corresponding to the resolution change (section 3.1).

2.2. Hovmöller plots

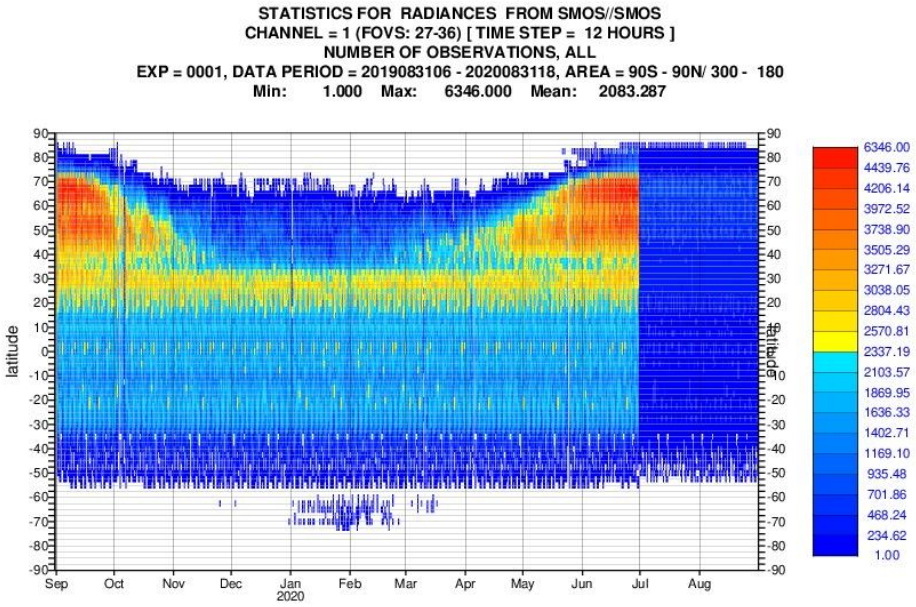

Figure 4: Hovmöller plot showing the number of SMOS observations monitored over land at 30° incidence angle, H polarisation covering 1st September 2019 to 31st August 2020

Statistics are plotted as a heat map with time on the x-axis and latitude on the y- axis for the twelve-month period with statistics accumulated in 2.5° latitude bins and 12 hour chunks. The statistics plotted are mean and standard deviation of first-guess departure, mean and standard deviation of observed value and number of observations. These plots allow local trends and jumps in the statistics to be identified. Figure 4 shows that the number of SMOS observations monitored over land varies significantly over the year. Between September 2019 and November 2019 the number of observations significantly reduces between 40°N and 80°N. As seen in the time series plots this is due to the Northern hemisphere winter and many observations at these latitudes being screened out due to frozen surfaces. The effect is enhanced at these latitudes because SMOS is in a polar orbit the swathes start to overlap near the poles therefore there are more observations in these areas than in the tropics. The opposite effect can also be seen between April 2020 and June 2020 as the Northern hemisphere summer begins. The number of observations over the tropics and Southern hemisphere varies far less over the year. Finally, the same reduction in observations can be seen from 30th June 2020 due to the resolution change.

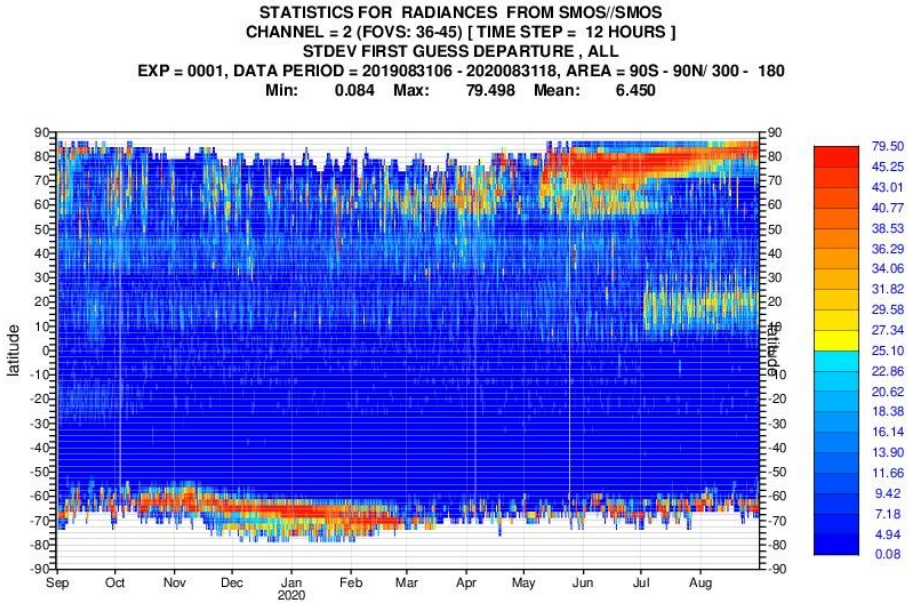

Figure 5: Hovmöller plot showing the number of SMOS observations monitored over ocean at 40° incidence angle, V polarisation covering 1st September 2019 to 31st August 2020

Figure 5 shows that between October 2019 and March 2020 between 55°S and 70°S there is an area of increased first-guess departures and a similar area between May 2020 and August 2020 between 70°N and 80°N. These are both due to the sub-optimal sea-ice screening and explain the increase in the global first-guess departures seen in figure 3. Also visible is an increase in first-guess departure between 10°N and 25°N from July 2020 onwards. This is related to a new, very strong RFI source in South-East China. The source is most likely over land, but it is strong enough that it contaminates SMOS observations over a wide region including over ocean. See section 3.3 for more details.

2.3. Maps

Due to the shift in statistics from June 30th 2020 the maps are accumulated from 1st September 2019 to 30th June 2020 and are plotted with longitude on the x-axis and latitude on the y-axis. The same statistics as for the Hovmöller plots are plotted. These plots allow an even more localised analysis of the statistics to be performed.

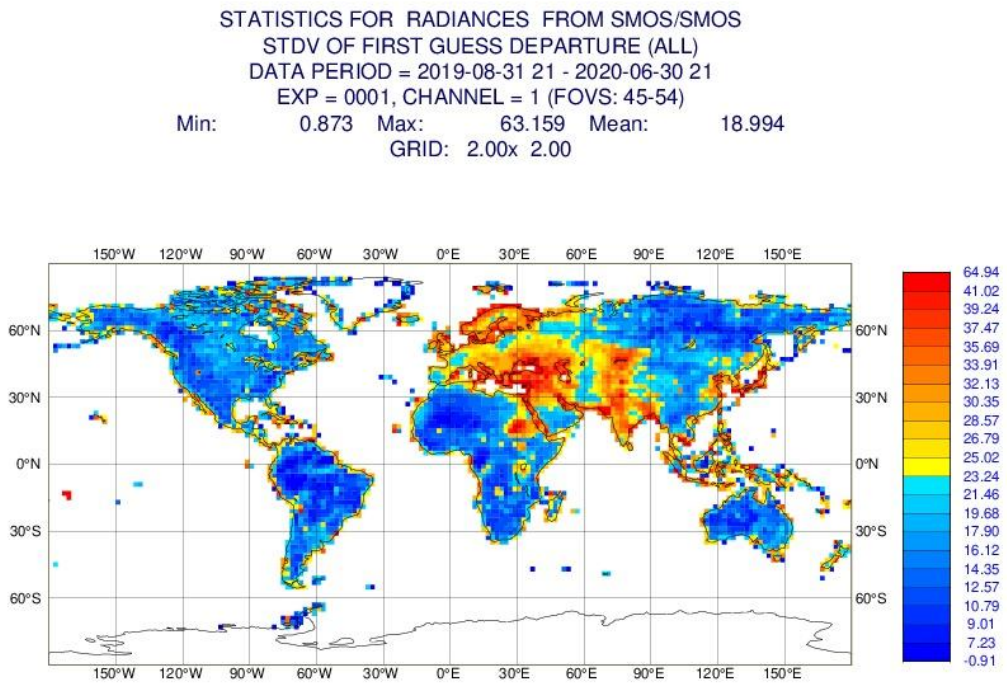

Figure 6: Map plot showing the standard deviation of SMOS first-guess departures over land at 50° incidence angle, H polarisation covering 1st September 2019 to 30th June 2020

Figure 6 shows largest first-guess departures over Europe, the Middle East, central Asia and Eastern Africa. This is caused by RFI in those regions and the signal from the RFI completely swamps any signal coming from changes in soil moisture. Figure 7 also shows that the contamination from RFI sources also extends over ocean with increase first-guess departures over the near-coastal areas of Europe and the middle East. This means it is very important to correctly screen out RFI, see sections 3.3 and 4.2 for more details.

Given the strong effects of RFI it is difficult to disentangle the variation in standard deviation of first guess departures caused by differing levels of RFI and natural variability. However, it can be seen from figure 6 that the first-guess departures are generally smaller over drier regions such as the Sahara desert, Western Australia and Siberia and larger over wetter regions such as central US and Canada, the Amazon and Eastern Australia. This is expected because the soil moisture will vary less in areas with low precipitation and will vary more in areas with higher precipitation. As mentioned above, differing levels of RFI in these regions could also be contributing to the differences seen in the plot.

Figure 7 also shows areas of increased first-guess departures over the Northern and Southern polar regions. This is again related to the sub-optimal sea-ice screening. In other areas there is very little variation in first-guess departures and this is because the observation operator CMEM treats the sea surfaces like lake surfaces. So there is currently no variation in simulated brightness temperature from waves or surface wind-speed as there will be in the observed brightness temperatures.

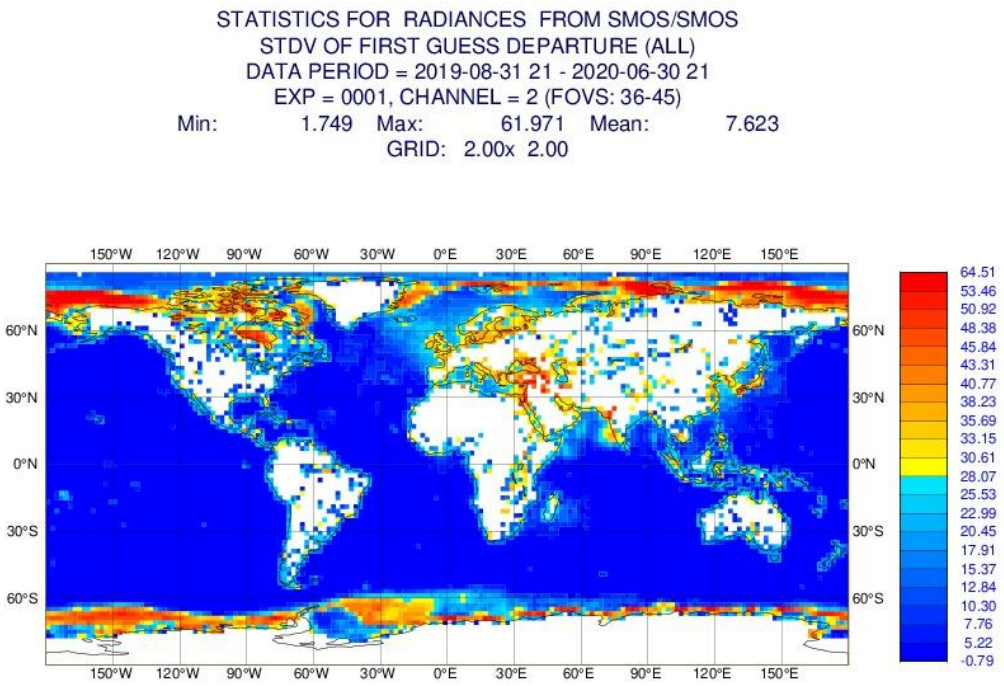

Figure 7: Map plot showing the standard deviation of SMOS first-guess departures over ocean at 40° incidence angle, V polarisation covering 1st September 2019 to 30th June 2020

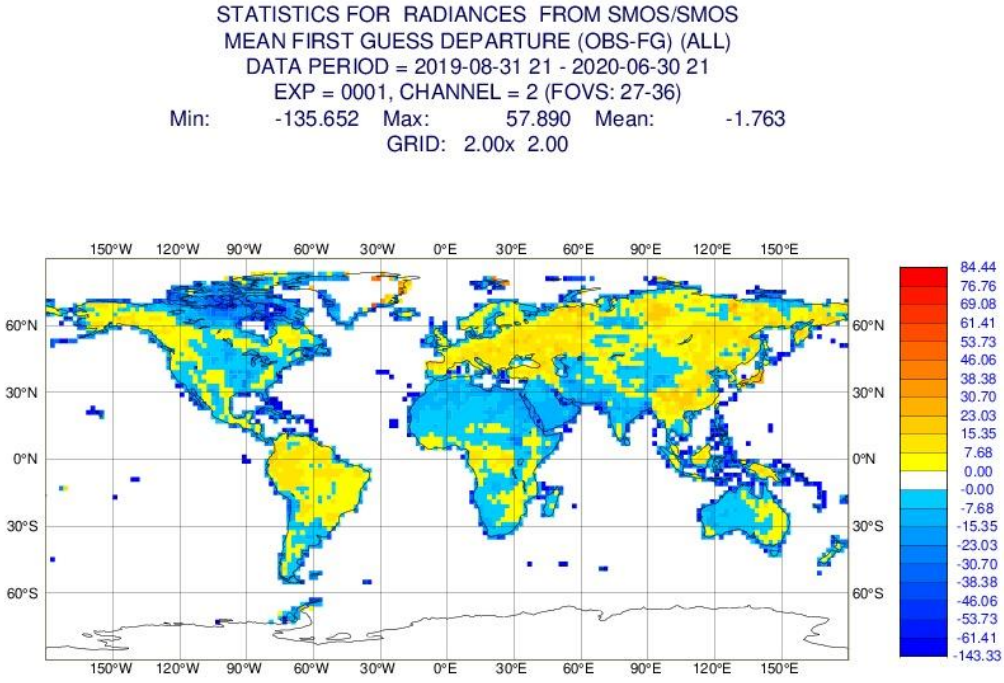

Figure 8: Map plot showing the mean of SMOS first-guess departures over land at 30° incidence angle, V polarisation covering 1st September 2019 to 30th June 2020

Figure 8 shows the global distribution of biases between the observations and the model equivalent values without any bias correction applied. There are positive biases over Europe, most of Asia and South America and negative biases over most of Africa, Australia and most of North America. Generally the negative biases seem to be located in drier regions indicating the model soil moisture is too dry compared to the observations. In the Northern hemisphere winter, observations in large areas over Northern Canada and Russia are screened out due to frozen surfaces. Observations in these areas are predominantly biased positive which then shifts the globally averaged biases negative. There are also strong negative biases over coasts which suggests that the coastal screening could be improved, see section 4.3 for more details.

2.4. Scatter

Statistics are accumulated from 1st September 2019 to 30th June 2020 and plotted as a 2-dimensional histogram with incidence angle on the x-axis and first-guess departure on the y-axis. These plots allow the distributions of first-guess departures at different incidence angles to be analysed.

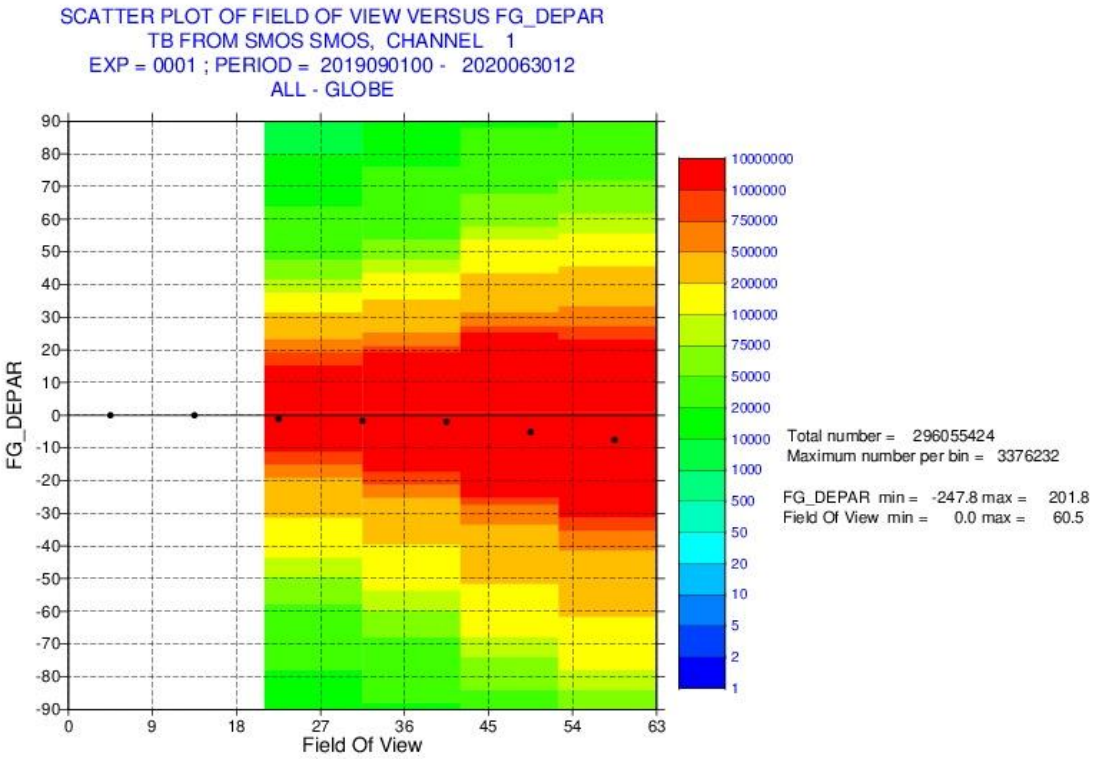

Figure 9: Scatter plot showing a 2D-histogram of SMOS first-guess departures over land for different incidence angle bins, H polarization covering 1st September 2019 to 30th June 2020. The black dots represent the mean first-guess departure for each incidence angle bin

Figure 9 shows that the distribution of first-guess departures is centred close to or just below zero for all incidence angle bins. It also shows that the histograms are close to symmetric with only a hint of a slightly larger negative tail in the histograms. This can be seen by looking at the number of

observations in the first-guess departure bins with a similar magnitude but opposite signs. Generally there are slightly more observations in the negative first-guess departure bins than the corresponding positive first-guess departure bins, especially at larger values, i.e. towards the tails of the distribution. This could be related to the sampling mentioned in section 2.3 and also the negative biases over coasts as seen in figure 8, see section 4.3 for more details.

3. Notable features in 2019/20

This section describes notable features which are visible in the monitoring plots for September 2019 to August 2020.

3.1. Change of resolution with 47r1 implementation on 30th June 2020

As seen clearly in figures 1 to 4 there was a significant reduction in the number of SMOS observations monitored from 30th June. This corresponds to the implementation of ECMWF cycle 47r1 which included a change to the model resolution that the SMOS monitoring runs with. Prior to June 2020 the model resolution was the same as the operational forecast resolution which is $T_{CO}1279$ (equivalent to a model grid point every ~9km). From June 2020 onwards the monitoring is now run at a resolution of T_L399 (equivalent to a model grid point every ~50km). There are a couple of reasons for this change: firstly, the lower model resolution better matches the SMOS field of view size (~50km) which leads to smaller errors of representation and interpolation when collocating the observations to the model locations; secondly, monitoring at lower resolution requires significantly fewer resources so it runs quicker and on fewer processors.

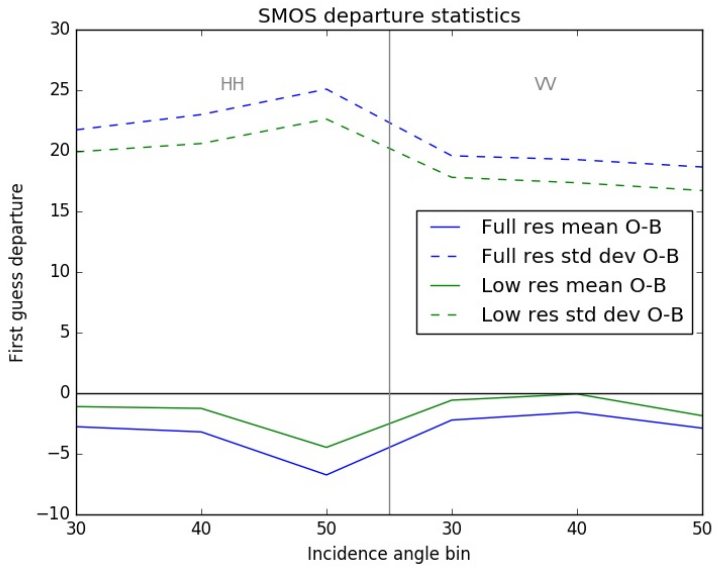

Figure 10: Mean (solid lines) and standard deviation (dashed lines) of SMOS first-guess departures when the monitoring is run at full ($T_{CO}1279$) resolution (blue) and lower (T_L399) resolution (green)

The reason this change results in a significant reduction in the number of SMOS observations monitored is because the first-guess departures are calculated at model locations. Lower model resolution means fewer model grid points which means fewer observations-model grid point match

ups. Another significant effect of this change is an improvement in both the mean and standard deviation of SMOS first-guess departures as can be seen in figure 10. Note that this improvement is hard to see in figures 1, 2, 3 and 5 due to the high day to day variability in the first guess statistics. Averaged over a longer period it can be seen that the mean first-guess departures are closer to zero and standard deviation of first-guess departures are smaller when running the monitoring at lower resolution. These effects are caused by the better match between the model and SMOS resolution leading to reduced errors of representation.

3.2. Sea-ice contamination in May 2020

In late May and early June 2020 there was a significant increase in the mean and standard deviation of first-guess departures over sea in the area between 70°N and 80°N, see figure 5. A similar increase can be seen between 60°S and 70°S between October 2019 and March 2020. Figure 7 also shows large standard deviation of yearly first-guess departures in both the Northern and Southern polar regions.

The time of the change coincides with a period of intense melting of Arctic/Antarctic sea-ice. Therefore, it seems that the cause of the change in the statistics was that the current frozen surface screening was not correctly flagging data in these areas at these times. It suggests that the 2 metre temperature was greater than 273K but that there was still sea-ice present. This would mean that the frozen surface check (for more details see Weston and de Rosnay, 2020) would not be triggered and first-guess departures for SMOS observations over sea-ice would be calculated and included in the statistics. The performance of CMEM over sea-ice is not as good as over non-frozen surfaces leading to the increased first-guess departures. See section 4.1 for possible solutions to this issue.

3.3. RFI

As discussed in Weston and de Rosnay (2020), the current RFI flagging used in the SMOS monitoring is inadequate and fails to correctly screen out many observations which are obviously contaminated by RFI. This can clearly be seen with the increased first-guess departures over Europe, the Middle East and Eastern Africa in figure 6.

The period covered by the statistics in figure 6 ended on 30th June 2020. Since early July 2020 a very strong RFI source has been detected in South-East China. The effect of this RFI source on the SMOS first-guess departures can be seen in figure 11. In June 2020 the first-guess departure statistics seem near-normal in South-East China whereas in July 2020 there is a large area of increased first-guess departures. There is also an area in mid-Asia around Kazakhstan where there are increased first-guess departures in June but near-normal statistics in July. This highlights how the strength and location of RFI sources can change on very short timescales.

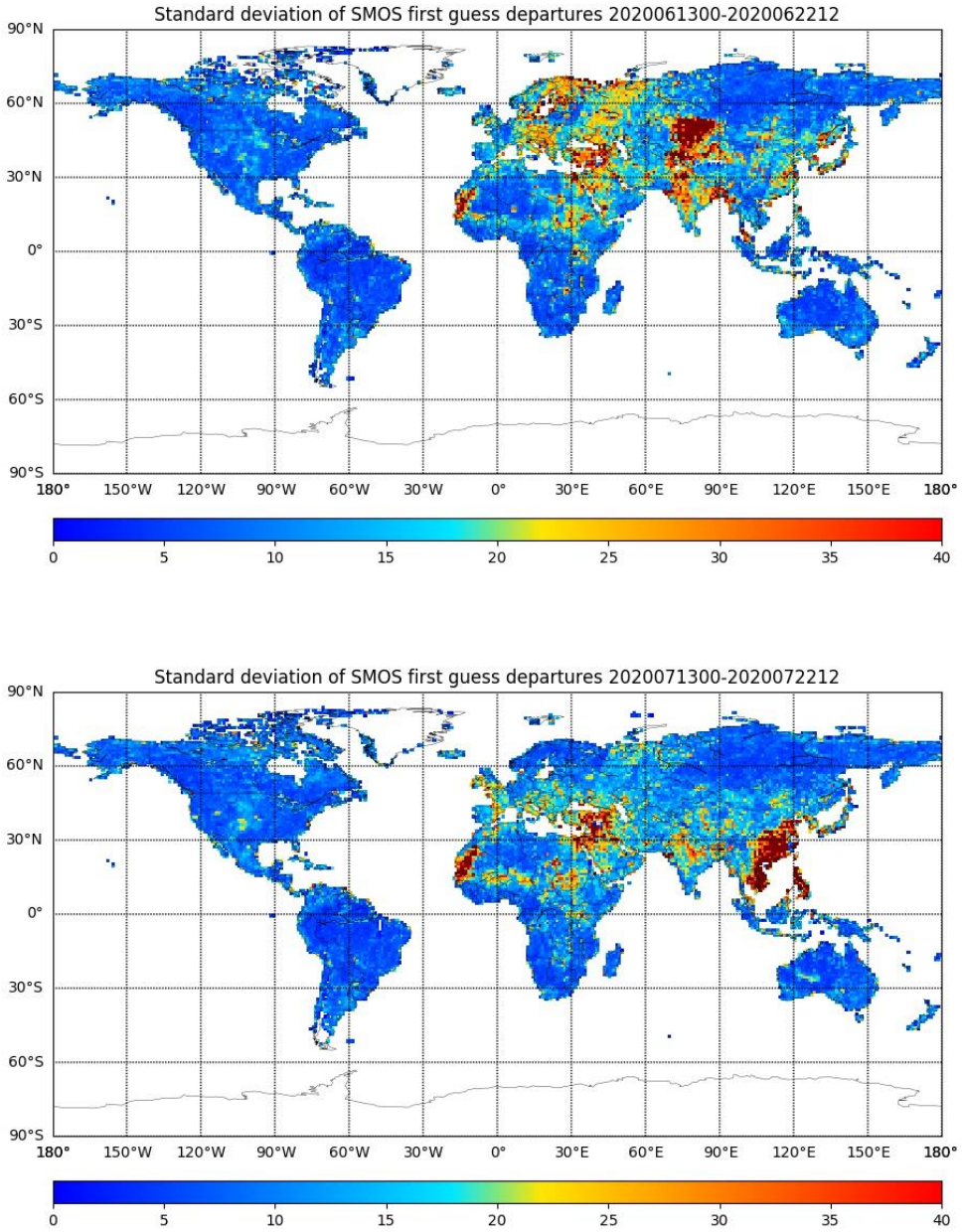

Figure 11: Map plot showing the standard deviation of SMOS first-guess departures over land at 40° incidence angle, H polarisation covering 13th June 2020 to 22nd June 2020 (top) and 13th July 2020 to 22nd July 2020 (bottom)

4. Future enhancements to the monitoring system

4.1. Frozen surface screening

As shown in section 3.2 the current frozen surface screening doesn't perform well during the melt season. This is because the current screening tests on whether there is a snow depth of >1cm and if the 2 metre temperature is greater than 273K. Over land this seems to perform adequately but over ocean

there are large areas where observations over sea-ice are allowed through and into the monitoring system.

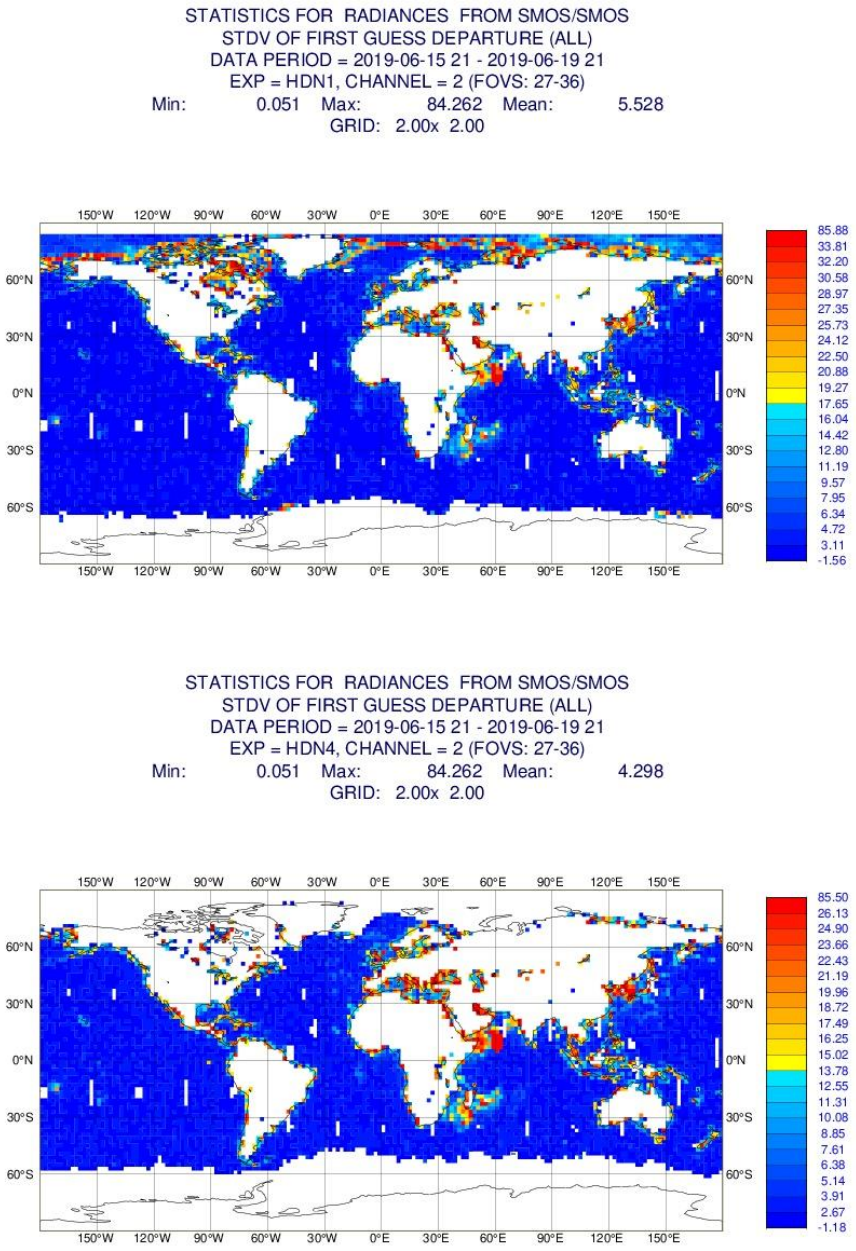

Figure 12: Map plot showing the standard deviation of SMOS first-guess departures over ocean at 30° incidence angle, V polarisation covering 15th June 2019 to 19th June 2019 with current frozen surface screening (top) and more conservative frozen screening (bottom)

Two possible solutions are proposed. Firstly, a more conservative threshold on the 2 metre temperature could be used. For the use of microwave radiances in the atmospheric analysis a threshold of 278K is used. An experiment using this threshold for SMOS was run in June 2019 and the areas of inflated first-guess departures at the sea-ice edge are indeed successfully screened out, see

figure 12. However, this also results in many more observations over land with 2 metre temperatures between 273K and 278K being screened out where the surface may not be frozen. A second approach would be to leave the existing 2 metre temperature threshold of 273K but add a test on the model sea-ice itself. This approach could be a more suitable solution for the identified problem and avoid the screening of many observations over non-frozen surfaces. This option will be tested in the next few months.

One of the above options will be implemented with the next ECMWF model cycle, 48r1.

4.2. RFI screening

As shown in section 3.3 of this report and section 3.2 of Weston and de Rosnay (2020) current RFI screening is sub-optimal and misses screening out many SMOS observations which are clearly affected by RFI. The current screening only uses the RFI flag in bit number 1 of the SMOS BUFR flag table (de Rosnay et al, 2015). However, there are additional flags in bit numbers 4 and 9 provided with the SMOS observations which can be used to more effectively screen out RFI. From September 2020 these flags are now included in the operational screening and separate plots with the screening turned on and off are now available on the monitoring web page. An example is shown in figure 13.

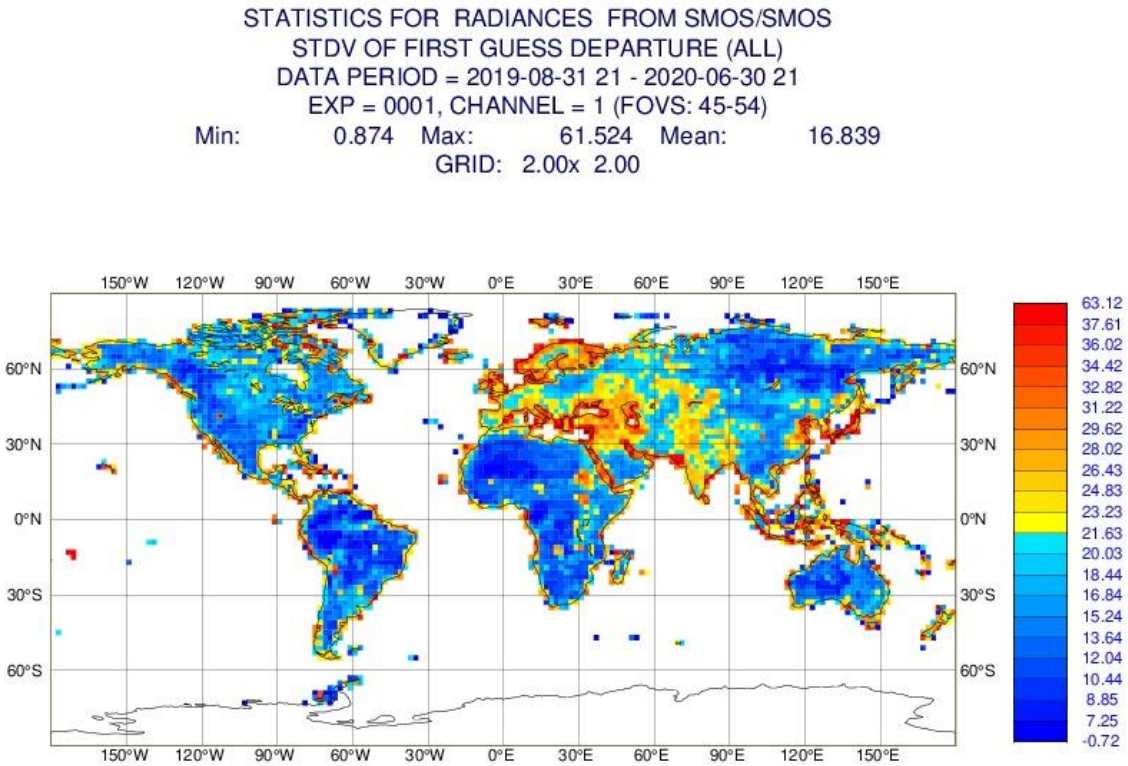

Figure 13: As figure 6 but with additional RFI screening turned on

Comparing figure 13 and figure 6 shows that the areas of increased first-guess departures have reduced. However, even with the new screening there are still areas of increased first-guess departures in areas of known RFI sources which shows that this screening is still not perfect. In addition, the extra screening

helps to mitigate the effects seen in figure 10 but doesn't completely remove the contaminated observations.

To help improve the RFI screening for SMOS there is ongoing work using potential new detection algorithms developed in the context of the ESA RFI4EO project led by Zenithal Blue Technologies. Improved RFI flags will be tested by analyzing SMOS first-guess departures in the ECMWF monitoring system. The aim is for this to enhance the RFI screening even further in the future.

4.3. Coastal screening

Currently observations where the closest model grid box contains 50% or more land are considered to be over land. This means many coastal areas and regions close to lake edges are considered to be land. As seen in figure 8 the mean first-guess departures are generally negative over coasts and lakes which contribute to skewing the overall distribution of the first-guess departures (figure 9). For assimilation of observations a Gaussian and symmetric distribution is assumed. Therefore, to enable assimilation better screening for coasts would be needed. For the assimilation of microwave radiances in the atmosphere a model grid box has to be covered by 95% land to be considered over land. Figure 14 shows that changing the coastal screening to use a threshold of 95% instead of 50% does reduce the negative tail as well as the positive tail and makes the distribution more Gaussian, especially near the centre. However, even with the more conservative coast screening the distribution is still biases negative which relates back to the sampling issues identified in section 2.3. More experiments will be run to test this enhanced coastal screening and it will be considered for implementation in the next ECMWF model cycle, 48r1.

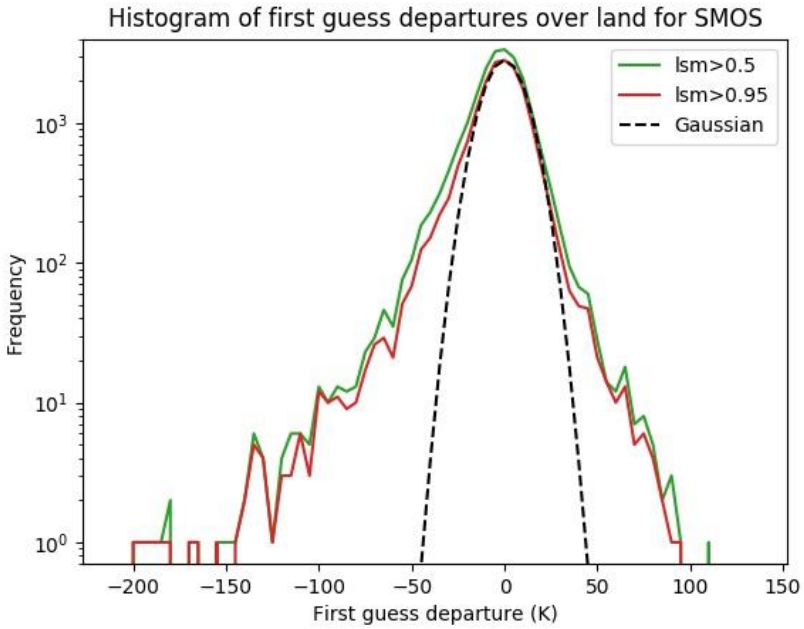

Figure 14: Histogram of first-guess departures using coastal screening with a land-sea mask > 50% (green) and land-sea mask > 95% (red)

4.4. Extended alias-free zone

The current SMOS monitoring only considers observations within the alias-free zone in the monitoring system. Any observations outside the alias-free zone are screened out in the pre-screening and hence first-guess departures are not calculated for these observations and they are not currently monitored. Figure 15 shows a SMOS snapshot with observations in the alias-free zone in green, observations in the extended alias-free zone in blue and observations in the border between the two in red.

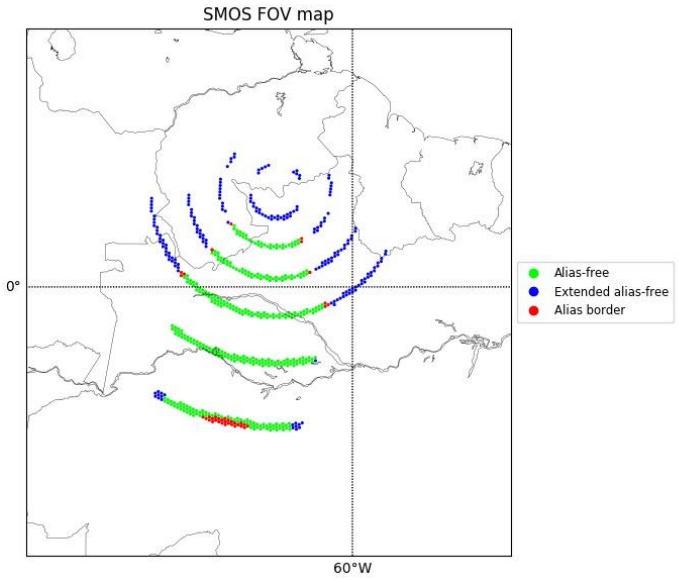

Figure 15: A SMOS snapshot from 22:15UTC on 16th June 2019 showing FOVs in the alias-free zone (green), alias border (red) and extended alias-free zone (blue)

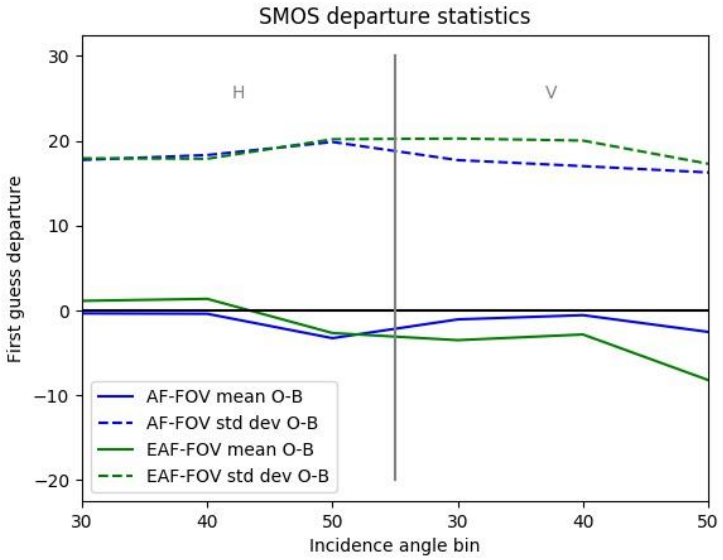

Figure 16: Mean (solid lines) and standard deviation (dashed lines) of SMOS first-guess departures for observations in the alias-free zone (blue) and the extended alias-free zone (green)

An experiment has been run to extend the monitoring to include observations from the extended alias-free zone by relaxing the existing check on bit number 5 of the NRT BUFR product within the pre-screening. The information on whether a given observation is in the alias-free zone or not is retained and then first-guess departure statistics have been calculated separately for those observations within the alias-free zone and those in the extended alias-free zone.

Figure 16 shows that the first-guess departure statistics are comparable for observations in the alias-free and extended alias-free zones. For the H polarisation the first-guess departure statistics are almost identical. For the V polarisation the mean first-guess departures are slightly more negative and the standard deviation of first-guess departures are slightly higher for the extended alias-free zone. It should be noted that, as illustrated in figure 15, there are very few observations in the extended alias-free zone with incidence angles around 50 degrees which means the statistics presented in figure 16 for this incidence angle bin are from a very small sample.

In light of these results it is proposed to additionally monitor SMOS observations in the extended alias-free zone operationally. This will be included with the next ECMWF cycle upgrade, 48r1. An additional filter will be added to the monitoring web page to allow monitoring plots for observations from the alias-free zone to be separated from plots for observations from the extended alias-free zone.

4.5. Yearly monitoring

Currently the time series and Hovmöller plots produced routinely and available on the ECMWF monitoring website are limited to the most recent 3 months period. This allows recent trends and changes to be identified. Plots covering longer periods can be produced manually (e.g. figures 1 to 5 in this report) but are currently not produced routinely. These are useful for identifying longer term trends and seasonal patterns. Therefore, it is proposed that yearly time series and Hovmöller plots will start to be routinely produced covering the period from July 2020 and the implementation of 47r1 and the monitoring resolution change to the present time. Currently these plots will largely overlap with the standard 3 monthly plots but as time goes on they will cover a longer and longer period.

It is also planned to develop multi-year monitoring using SMOS reprocessed NRT Tb from 2010 onward (de Rosnay and Weston, 2019). This activity will be conducted in 2021-2022 in context of the ESA SMOS-E. The SMOS multi-year reprocessed data monitoring will be complementary to the current operational monitoring.

References

de Rosnay, P., M. Dragosavac, M. Drusch, A. Gutiérrez, M. Rodríguez López, N. Wright, J. Muñoz Sabater, Raffaele Crapolicchio: SMOS NRT BUFR specification, 2015. https://earth.esa.int/documents/10174/1854583/SMOS_NRT_BUFR_Specification

de Rosnay P. and P. Weston: SMOS long-term assessment based on re-analyses: strategy and work plan", ESA contract report. ESA SMOS-E contract 4000125399/18/I-BG, December 2019

de Rosnay, P., J. Muñoz-Sabater, C. Albergel, L. Isaksen, S. English, M. Drusch, J.-P. Wigneron: SMOS brightness temperature forward modelling and long term monitoring at ECMWF. Remote Sens. Environ., 237 (2020): 111424. https://doi.org/10.1016/j.rse.2019.111424

Weston, P., P. de Rosnay: Quality control plan for brightness temperature monitoring. ESA contract report. SMOS ESL contract 4000130567/20/I-BG, July 2020